PCCP

Accepted Manuscript

ROYAL SOCIETY OF CHEMISTRY

www.rsc.org/pccp

Graphdiyne as a metal-free catalyst for low-temperature CO oxidation

Ping Wu, Pan Du, Hui Zhang, and Chenxin Cai*

Jiangsu Key Laboratory of New Power Batteries, Jiangsu Collaborative Innovation Center of Biomedical Functional Materials, College of Chemistry and Materials Science, Nanjing Normal University, Nanjing 210097, P. R. China.

* Corresponding author, E-mail: cxcai@njnu.edu.cn (C. Cai)

Electronic supplementary information (ESI) available: Comparison of the configurations of the CO and O_2 adsorbed on graphdiyne surface obtained from CASTEP code and DMol3 code, optimized configuration, band structure, and distribution of charge density of 3 × 3 supercells of graphidiyne, and configurations of each state and minimum energy profiles for CO oxidation reaction on graphdiyne sheet along pathway I in ER mechanism.

ABSTRACT: The oxidation of CO has attracted great interest in recent years because of its important role in enhancing the catalyst durability in fuel cells and in solving the growing environmental problems caused by CO emission. The usually used noble metal nanocatalysts are costly and require high reaction temperature for efficient operations. We report here a density functional theory (DFT) study of low-temperature CO oxidation catalyzed by graphdiyne, which is a new two-dimensional periodic carbon allotrope with a one-atom-thick sheet of carbon building of sp- and sp^2-hybridized carbon atoms and has been shown in our recent work to have high catalytic activity for oxygen reduction reactions (ORRs). We studied the adsorption properties of CO and O_2 on graphdiyne, simulated the reaction mechanism of CO oxidation involving graphdiyne, and analyzed electronic structures of each step in reaction progress. The simulation results indicate that the adsorption of O_2 prevails over CO adsorption on graphdiyne sheet; the reaction of CO oxidation by adsorbed O_2 on graphdiyne proceeds via the Eley-Rideal (ER) mechanism with a decrease in the energy of the system and the energy barrier of as low as 0.18 eV in the rate-limiting step. The oxidation reaction includes the breakage of the O–O bond in the adsorbed O_2, formation of the metastable carbonate-like intermediate state, and the creation of CO_2 molecules. The results presented here demonstrate that the graphdiyne is a good, low-cost, and metal-free catalyst for low-temperature CO oxidation and can be used to solve environmental CO emission and in fuel cell with high ability of CO tolerance by its oxidation removal.

Keywords: CO oxidation; Metal-free catalyst; Carbon materials; Graphdiyne.

1. Introduction

Fuel cells have received much attention because of their high energy conversion efficiency, low pollution, low operating temperature, high power density, and wide range of applications.[1,2] Pt and Pt-based materials are still the most common catalysts used to promote the cathodic oxygen reduction reactions (ORRs) and/or anodic alcohol oxidation reactions (AORs) in fuel cells,[3-9] but several problems exist with Pt-based catalysts including limited natural resources, high cost, toxic CO-like intermediate species, and sluggish ORR kinetics. Among them, CO poison has long been regarded as a big challenge of the Pt-based catalysts because even a trace amount of CO can significantly block the catalytic sites of the Pt-based catalysts due to its strong adsorption on the catalyst surface (the binding energy of CO at Pt surface is 1.49–1.8 eV,[10] while the binding energy of H_2 (a fuel in fuel cells) is 0.7–0.83 eV[11]), resulting to a sluggish kinetics, a high overpotential (usually more than 0.7 V for H_2 oxidation), and a significant degradation in the catalytic activity of those catalysts (note that very recent studies also show that the adsorbed CO can enhance the binding of OH to the surface of catalyst.[12-14] The adsorbed OH can promote the oxidation of CO in solution.[12] Moreover, the CO-promoted adsorption of OH may lead to the oxidation of other species in solution such as HCOOH[13] and alcohol molecules[14]). In addition, CO is commonly generated during the fuel refining and in the oxidation of organic fuels, and presents in the fuel gas at a level of ~0.5–2%.[15] Thus, designing a catalyst with a high ability of CO-tolerance is critical to the development of fuel cells for commercial applications. An efficient way to achieve this goal is to remove CO from catalyst surface by its oxidation. Therefore, the exploration of catalysts with high catalytic activity to CO oxidation is very significant. Moreover, the reaction of CO oxidation also plays an important role in solving the growing environmental problems caused by CO emission from automobiles and industrial processes, and is often regarded as an important prototype reaction for designing the atomic-scale catalysts.

Earlier studies indicated that some noble metals (such as Pd,[16,17] Au,[18] and Rh,[19] etc.) exhibited high activity of CO oxidation, they are however costly and require high reaction temperature for efficient operations (> 100 °C), impeding their general use. Recent studies addressed that the low-cost non-noble

metal based catalyst such as the iron cluster,[20] and the oxide cluster of iron[21] and cobalt[22] showed the high activity for low-temperature CO oxidation. Substrates may also enhance the stabilities and improve the catalytic properties of catalysts. In this regard, graphene has been chosen as a substrate for metals (Fe,[23,24] Cu,[25] and Ni[26]), and such systems demonstrated high activity for CO oxidation at an ambient temperature. For example, Li et al.[23,24] recently showed good catalytic activity of the Fe-embedded (where one carbon atom of the graphene hexagonal lattice is substituted by an Fe atom) for CO oxidation. DFT calculation demonstrated that the improved catalytic activity was attributed to the positive charged Fe atom resulted from charge transfer (~0.27 au) from Fe to graphene in the formation of Fe-embedded graphene.[23] This positive charged Fe atom has a strong adsorption capability for O_2, which could interact with and oxidize CO molecules. Thus, the generated Fe atom acts as a catalytic site for CO oxidation. Song et al.[25] obtained the similar conclusions in the case of Cu-embedded graphene.

In search of low-cost and high-activity catalysts for CO oxidation, the non-metal-doped carbon materials (such as carbon nanotube, carbon nanofiber, and graphene)[27-32] have also attracted particular attention as metal-free catalysts. For example, the vertically aligned nitrogen-doped carbon nanotubes (VA-NCNTs) have high CO-tolerance ability and could actively catalyze ORRs via a high efficient four-electron process without crossover effects.[31] The high CO-tolerance ability of VA-NCNTs was attributed to the electron accepting nature of the doped nitrogen atom, which breaks the intrinsic eletroneutrality of CNTs and creates a net positive charge (via intramolecular charge-transfer) on the adjacent carbon atoms to readily facilitate O_2 adsorption. The adsorbed O_2 will then react with CO and remove CO through oxidation process, and thus offer high CO resistance. In contrast with the nitrogen-doped CNTs in which the carbon atoms adjacent to the nitrogen dopant are positive charged, in boron-doped CNTs (BCNTs),[32] the boron dopant itself is positive charged because carbon has a larger electronegativity than boron inducing a significant positive charge on the boron atom. This positively charged boron atom can also favorably capture O_2 molecule, which will then react with CO and remove CO through oxidation process. These investigations provide a good understanding the activity of the catalyst to CO oxidation that the positive charged sites (the metal atoms on metal-embedded graphene,

the carbon atoms adjacent to the nitrogen dopant in NCNTs, or the boron atoms in BCNTs) play a key role in catalytic oxidation of CO.

Thus, graphdiyne, a new two-dimensional carbon material with a one-atom-thick layer of carbon built from triple- and double-bonded units of two sp– and sp^2–hybridized carbon atoms, is a good candidate for metal-free catalyst of CO oxidation because our previous work indicated that the charge distributions on graphene (belongs to the same family as graphdiyne) surface are not even: some carbon atoms have a net positive charge caused by charge transfer at graphene sheet.[33] In that study, we demonstrated that these positively charged sites can improve the interaction between graphene and O_2 molecules and facilitate the ORR process.[33] To demonstrate whether the graphdiyne has a catalytic activity to CO oxidation, we reports a DFT study of low-temperature CO oxidation involving graphdiyne (note that graphdiyne has a high possibility of synthesis because large area (~3.6 cm^2) films of graphdiyne have been successfully prepared via a cross-coupling reaction using hexaethynylbenzene on a copper surface[34]). The simulation results suggest that graphdiyne can be a good, low-cost catalyst for low-temperature CO oxidation and could be used in solving environmental CO emission and in fuel cells with high CO tolerance ability by its oxidation removal.

2. Calculation details

Our calculations were performed using spin-polarized density functional theory (DFT) as implemented in CASTEP code. The exchange-correlation energy function of the Perdew-Burke-Ernzerhof (PBE) version of the generalized gradient approximation (GGA)[35] with Grimme methods for DFT-D correction was used. The plane-wave basis set was truncated at a kinetic energy cutoff of 380 eV, which allows convergence to 0.5×10^{-6} eV in total energy. In the calculation, we performed the geometric optimization using the constrained unit-cell parameters and the optimization was considered convergence when the spring force between adjacent images was less than 0.01 eV/Å, the total energy change upon two steps for the electronic self-consistent field iteration was less than 0.5×10^{-6} eV, and the total stress tensor was reduced to the order of 0.05 GPa.

The primitive cell of graphdiyne containing of 18 carbon atoms (Fig. 1) was used as a model system. The modulus unit cell vector in the z direction was set to be 20 Å, which led to negligible interactions between the system and their mirror images. For geometric optimization and the search for the transition state (TS), the Brillouin zone integration was performed with 3 × 3 × 1 k-point sampling according to the Monkhorst-Pack scheme,[36] which brought out the convergence tolerance of energy of 1.0×10^{-5} hartree and that of maximum force of 0.002 hartree. For the density-of-states (DOS) calculation, the k-point mesh was also set to 3 × 3 × 1 because increasing the k-points mesh to 7 × 7 × 1 did lead to negligible energy differences, implying that 3 × 3 × 1 is enough to achieve high accuracy for DOS calculation.

In study of the adsorption of CO, O_2, or CO and O_2 co-adsorption, we optimized the geometric structure of the adsorbed graphdiyne and calculated the charge transfer upon adsorption via Mulliken charge density analysis. The adsorption energy (E_{ad}) for these molecules on graphdiyne is defined as:

$$E_{ad} = E_t - E_0 - E_x \quad (1)$$

where E_t, E_0, and E_x are the total energy of the total adsorbed system including the adsorbed molecules and graphdiyne, the isolated molecules (CO, O_2), and the graphdiyne, respectively. By this definition, a negative value of E_{ad} denotes an exothermic adsorption process, implying that the adsorption of adsorbate molecules on graphdiyne surface is energetically favorable, while a positive value of E_{ad} denotes an endothermic adsorption process, implying that the adsorption of the adsorbate molecules on graphdiyne surface is energetically unfavorable.

To investigate the minimum energy pathway (MEP) for CO oxidation, linear synchronous transit (LST/QST) and nudged elastic band (NEB) tools in DMol^3 code were used,[37,38] which have been proved to be the efficient method for finding the MEP between the given initial and final state of a transition state and can improve calculation efficiency significantly in comparison with CASTEP code. More importantly, the configurations of the CO and O_2 adsorbed on graphdiyne surface obtained from DMol^3 code are in the same as those obtained from CASTEP code (the configurations of the adsorbed CO and

O_2 obtained from DMol[3] code and CASTEP code are presented in Fig. S1, ESI). Frequency calculation was also performed to search for MEP and determine the transition state (TS) for CO oxidation.

3. Results and discussion

For calculation, we constructed the primitive cell of graphdiyne containing of 18 carbon atoms as a model system (Fig. 1). To make certain that our computational approach is appropriate, we first optimized the configurations of graphdiyne (Fig. S2a, b, ESI). The optimized cell parameter of graphdiyne is 9.46 Å, the mean C–C bond length in hexagon is 1.42 Å, the C–C and C≡C bond length in the diacetylenic links is 1.39 and 1.22 Å, respectively, agreeing well with those reported previously (1.39 and 1.22 Å for C–C and C≡C, respectively).[39-41] Furthermore, the valence band and the conduction band in graphdiyne are along the Γ point and their band gap is calculated to be 0.53 eV (Fig. S3, ESI), which is consistent with the earlier reports (0.53 eV).[39,42] These results imply that the model we constructed is reasonable. Vibration analysis confirms that the optimized configuration is stable. The bond length of isolated (in gas-phase) O_2, CO, and CO_2 is predicted to be 1.22 Å (O–O for O_2), 1.14 Å (C–O for CO), and 1.17 Å (C–O for CO_2), respectively, in a 10 × 10 × 10 $Å^3$ cubic box, which are in good agreement with available experimental data and theoretical results (1.21 Å for O–O of O_2;[43] 1.15 Å for C–O of CO;[44] 1.16 Å for C–O of CO_2).[45] These results further demonstrate that our calculations are appropriate.

Before characterizing the adsorption of O_2 or CO on graphdiyne, we simulated the charge distribution on each carbon atom in graphdiyne sheet through Mulliken charge density analysis because the charge distribution on carbon atoms is important for finding the adsorption sites on graphdiyne sheet. The distribution of the charge density on graphdiyne sheet is not uniform because of the localization of the π electrons, which is due to the presence of the –C≡C– groups in the construction of the units of graphdiyne (Fig. S2b, ESI). We find that there is an electron transfer from the sp hybridized carbon atoms in the diacetylenic link to the sp^2 hybridized carbon atoms in the hexagonal ring (C_6 ring), resulting that the sp^2 carbon atoms are negative charged while the sp hybridized carbon atoms around the C_6 ring and in the diacetylenic-like rods are positive charged. This could be clearly observed from

the charge density plots of graphdiyne (Fig. S4, ESI). The electron deficient nature of the carbon atoms around the C_6 ring and in the diacetylenic-like rods will favor the O_2 or CO adsorption through the electron transfer from the adsorbates to carbon atoms in graphdiyne because our previous work had shown that the positive charged sites on graphyne (18,18,18-graphyne) surface could act as the binding sites for O_2.[33]

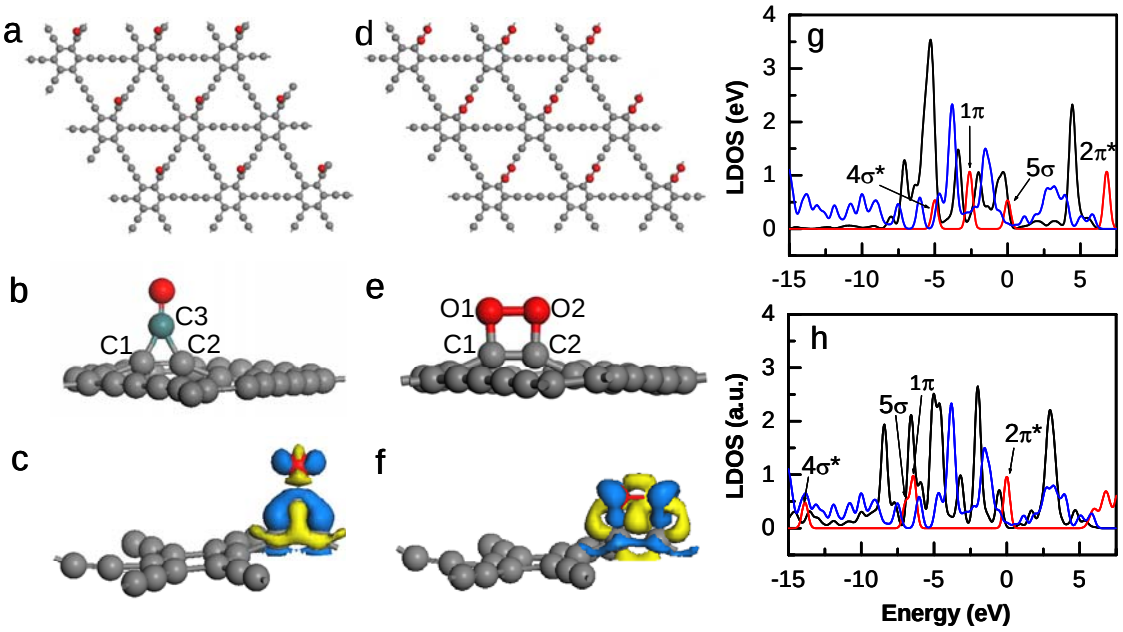

Fig. 1 Top (a, d) and side (b, e) views of optimized configurations, and electron density difference maps (c, f) of CO (a, b, c) and O_2 (d, e, f) adsorbed on graphdiyne sheet. Atomic color code: gray, carbon; red, oxygen; and green, carbon atom of CO molecule. The blue and yellow color in (c) and (f) represents increasing and decreasing electron density, respectively. (g) depicts the local density of states (LDOS) projected onto C–O for the isolated CO (red line) and the adsorbed CO (black line). The blue line in (g) shows the LDOS projected onto C atoms in graphdiyne bound with adsorbed CO. (h) depicts the LDOS projected onto O–O for the isolated O_2 (red line) and the adsorbed O_2 (black line). The blue line in (h) shows the LDOS projected onto C atoms in graphdiyne bound with adsorbed O_2.

We then studied the adsorption properties of O_2, CO, and CO_2 on graphdiyne sheet. We examined several possible adsorption sites (such as the sp^2 hybridized carbon atoms in C_6 ring, the sp hybridized carbon atoms around the C_6 ring, and the sp hybridized carbon atoms in the diacetylenic-like rods) in order to find out the energetically most stable configuration for each adsorbate. It was found that the CO and O_2 were only adsorbed on the sp hybridized carbon atoms, not adsorbed on the sp^2 hybridized

carbon atoms. For CO adsorption, we started by placing a CO molecule at a distance of 3 Å above the graphdiyne plane and optimized the configurations. The most favorable structure adopts an end-on configuration (in which the O–C bond points to the sp hybridized carbon atom) (Fig. 1a, b). Two sp hybridized carbon atoms (C1 and C2) in graphdiyne sheet rise out of the plane and form a triangle with the carbon atom of the adsorbed CO (Fig. 1b), implying the formation of two C–C chemical bonds between the carbon atoms of adsorbed CO and graphdiyne. The bond length of C1–C3 and C2–C3 is 1.429 Å and 1.455 Å, respectively, further verifying the formation of the C–C chemical bond between CO and graphdiyne. This configuration is significantly different from those for the CO adsorption on the metal-embedded (such as Fe-,[23] and Cu-embedded[25]) or metal-anchored (such as Fe-anchored[24]) graphene. In those cases, CO was adsorbed on the embedded metal atom with a title angle perpendicular to the metal-graphene substrates and only one chemical bond (C–metal) was formed between the carbon atom of adsorbed CO and the embedded metal atom.

The adsorption energy for the CO adsorption on graphdiyne sheet (E_{ad}(CO)) is calculated to be about –1.43 eV (please refer to the section of calculation details for the definition of the adsorption energy), and there is about 0.05 au charge transfer from graphdiyne to CO, which occupies the antibonding CO-2π* orbital and subsequently leads to a slight elongation of C–O bond (l_{C-O}) to 1.22 Å from 1.14 Å. These electrons not only accumulate on the O atom but also on C–C bond (Fig. 1c). However, the whole graphdiyne structure remains covalent (Fig. 1a).

For O_2 adsorption on graphdiyne sheet, the most energetically favorable configuration is characterized by O_2 parallel to graphdiyne plane (side-on mode) (Fig. 1d, e). This side-on configuration for the O_2 adsorption on graphdiyne agrees well with those previous reports for O_2 adsorption on graphyne,[33] on nitrogen-doped graphene,[46] and on boron or nitrogen-doped carbon nanotube.[31,32] Following the adsorption, the graphdiyne plane distorts into a saddle-shaped surface while the C1 and C2 rise out of the plane to form a tetrahedral structure (Fig. 1e), which is indicative of the formation of the C–O chemical bonds. The distances between the C1 and O1 and the C2 and O2 are reduced to 1.41 Å (C1–O1) and 1.43 Å (C2–O2), respectively, from an initial value of 3 Å, further indicating the

formation of two new C–O bonds and the strong adsorption of O_2 on graphdiyne. Accompanied by the adsorption, there is about 0.41 au charge transfer from graphdiyne to O_2, which occupies O_2-2π* orbital and brings out an obvious elongation of O–O bond ($l_{O–O}$) to 1.49 from 1.22 Å, implying an effective weakening of O–O bond. The remarkable electron transfer can be also observed from electron density difference map as shown in Fig. 1f, which shows that the electron mainly accumulates on O_2 molecule. The whole graphdiyne structure is still covalent (Fig. 1d), similar to the case of the CO adsorption on graphdiyne sheet (Fig. 1a). This charge accumulation is in good agreement of the elongation of O–O bond since the more charge transfers to O_2 from the graphdiyne, the more the O–O bond elongates.

The predicted adsorption energy of O_2 ($E_{ad}(O_2)$) on graphdiyne is about –3.27 eV, which is much higher than that for the end-on configuration of CO adsorption (–1.43 eV). The value of $E_{ad}(O_2)$ for O_2 adsorption on graphdiyne is also significantly higher than those obtained for O_2 adsorption on Pt(111) (–0.58 to –0.72 eV),[47] Pt(001) (–1.30 eV),[48] Pt(110) (–1.48 eV),[49] Pt_2 (–1.42 eV),[50] Pt_3 (–1.08 eV),[51] Au_7 and Au_9 (about –0.5 eV),[52] and Au_4 cluster (–0.24 eV),[51] Fe- (–2.09 eV),[23] Au- (–1.34 eV),[52] and Cu-embedded graphene (–2.67 eV),[25] and Pd(111) (0 eV),[51] suggesting the high adsorption ability of O_2 on graphdiyne sheet. This strong ability of graphdiyne for O_2 adsorption will greatly benefit to its high electrocatalysis performance in fuel cell (such as toward ORRs) as well as to its high resistance to CO poison because stable adsorption of O_2 is necessary for ORRs and for removal of CO via its oxidation reaction. Meanwhile, the significant distortion of graphdiyne sheet caused by the strong adsorption of O_2 also provides more degrees of freedom for reaction sites. Note that, similar to the case of graphyne, the adsorption of O_2 on graphdiyne sheet cannot result to the oxidation of graphdiyne.

To gain the deeper insight into the interaction between graphdiyne and the adsorbed CO and O_2, the local density of states (LDOS) projected onto C–O and O–O and LDOS of isolated CO and O_2 molecule were analyzed and compared (Fig. 1g, h). For the CO adsorption on graphdiyne sheet, the antibonding 2π* orbital of C–O is unoccupied (Fig. 1g), agreeing well with the electron density difference mapping (Fig. 1c). There is almost no hybridization between CO-2π* orbitals near the Fermi level and s and p orbitals of graphdiyne, while the top occupied 5σ orbital in the isolated CO molecule shifts below the

Fermi level and hybridizes with orbital of graphidyne, agreeing well with that predicated by Hammer-Nørskov mode,[53] which concluded that, in adsorbate-metal bonding case, the charge transfer from the s and p orbitals of metal to the adsorbate result to a broadening of the valence states of adsorbate. The broadened valence states further hybridize with the localized d states of metal. This hybridization results a slight increase in C–O bond length (~0.08 Å) as evidenced from Fig. 1b. In the case of the O_2 adsorption on graphdiyne sheet, however, the antibonding $2\pi^*$ orbital of O_2 is fully occupied and pulled below the Fermi level (Fig. 1h), which weakens the O–O bond and promotes the formation of C–O bonds. Meanwhile, 1π and 5σ orbitals of O_2 become broadened and hybridize with the orbital of graphdiyne, inducing the elongation of O–O bond. However, the antibonding O_2-$4\sigma^*$ orbital does not hybridize with the orbital of graphdiyne due to its energy far below the Fermi level. Therefore, in contrast to the slightly increased C–O bond length after adsorption, the O–O bond length of the adsorbed O_2 molecule is significantly elongated by about 0.27 Å. This difference is caused by the different occupations of antibonding $2\pi^*$ orbitals of O_2 and CO and the different hybridization extent of those orbitals with graphdiyne, resulting from a more significant charge transfer from graphdiyne to the antibonding $2\pi^*$ orbitals of O_2 in comparison with that of CO adsorption (the charge transfer from graphdiyne to O_2 and CO is 0.41 and 0.05 au, respectively).

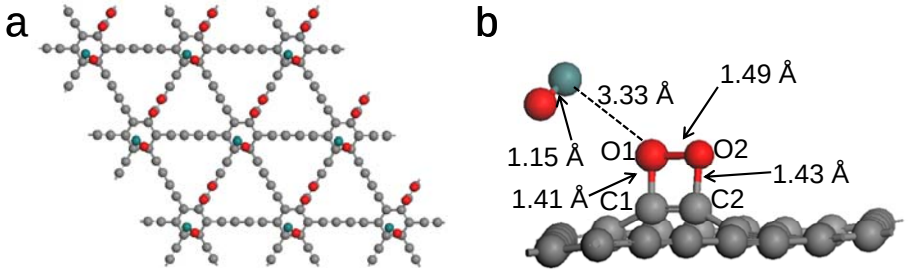

Fig. 2 Top (a) and side (b) views of optimized configurations of O_2 and CO co-adsorbed on graphdiyne sheet. Atomic color code: gray, carbon; red, oxygen; and green, carbon atom of CO molecule.

For the CO_2 molecules, we also studied various possible adsorption sites and found the most stable adsorption site also locates on the sp hybridized carbon atoms of the graphdiyne plane with CO_2 molecule perpendicular to the graphdiyne plane. The distance of the O atom in CO_2 molecule to the

graphdiyne sheet is ~3.37 Å and the $E_{ad}(CO_2)$ is –0.04 eV, suggesting that a CO_2 molecule is weakly adsorbed on graphdiyne sheet and can easily be desorbed from the reaction site at ambient temperature.

We also studied the co-adsorption of O_2 and CO molecules on graphdiyne sheet. Our calculation revealed that the co-adsorption process is an exothermic process with $E_{ad}(CO+O_2)$ = –3.33 eV, which is only slightly higher than that of O_2 ($E_{ad}(O_2)$ = –3.27 eV) and is much less than the sum of O_2 and CO adsorption energies (–4.70 eV), indicative of a strong repulsion between the adsorbed O_2 and CO molecules. Thus, it seems hard to form the OOCO intermediate state, which can be evidenced from the optimized configuration of co-adsorption of O_2 and CO on graphdiyne (Fig. 2a, b). In this optimized configuration, O_2 bonds with graphdiyne in a side-on mode with formation of two C–O bonds with bond length of 1.41 (C1–O1) and 1.43 Å (C2–O2), respectively. However, there is no chemical bond formed between the adsorbed CO and graphdiyne, and CO molecule is rather separated from the adsorbed O_2 molecule with a distance of 3.33 Å (from the C atom in CO to the O1 atom in O_2 molecule, Fig. 2b). Upon adsorption, there is about 0.42 au charge transfer from graphdiyne to O_2 and no charge transfers to CO, suggesting the strong adsorption of O_2 on graphdiyne sheet and the weak one of CO. The O–O bond length increases significantly by 22% respect to the isolated O_2 molecules (from 1.22 to 1.49 Å), indicating the activation of O_2 upon the adsorption on graphdiyne. In contrast, the C–O bond length remains nearly unchanged in comparison with its isolated state (from 1.14 to 1.15 Å). Therefore, from the adsorption energy point of view, the adsorption of O_2 is preferred than that of CO on graphdiyne sheet, and graphdiyne surface will be covered with O_2 if CO and O_2 co-existed in the system. The natures of the co-adsorption of O_2 and CO will affect the mechanism of CO oxidation at graphdiyne sheet.

Having characterized the adsorption of CO and O_2 on graphdiyne sheet, we studied the reaction mechanism of CO oxidation on graphdiyne. Generally, there are two well-established mechanisms for CO oxidation with O_2, namely, Langmuir-Hinshelwood (LH) mechanism and Eley-Rideal (ER) mechanism.[23,25,52] The LH mechanism involves the co-adsorption of CO and O_2 molecules on the catalyst surface before reaction, reaction of the co-adsorbed CO and O_2 molecules, formation of a

peroxo-type complex intermediate (OOCO), which is the rate-limiting step, and desorption of the generated CO_2 molecule from catalyst surface. In the ER mechanism, the CO molecules directly react with the adsorbed and activated O_2, i.e., the adsorbed atomic O, where the activation of O_2 is the rate-limiting step. Since the adsorption of O_2 on graphdiyne is 1.84 eV more favorable than the case of CO adsorption, and the $E_{ad}(CO + O_2)$ is only slightly higher than that of O_2, there is a strong repulsion between O_2 and CO molecules. It is hardly to generate peroxo-type complex intermediate. In contrast, the dissociative adsorption of O_2 is energetically favorable on graphdiyne sheet. Therefore, the ER mechanism is expected to prevail over the LH mechanism for CO oxidation on graphdiyne sheet. For a comprehensive understanding, we discuss both mechanisms in this study.

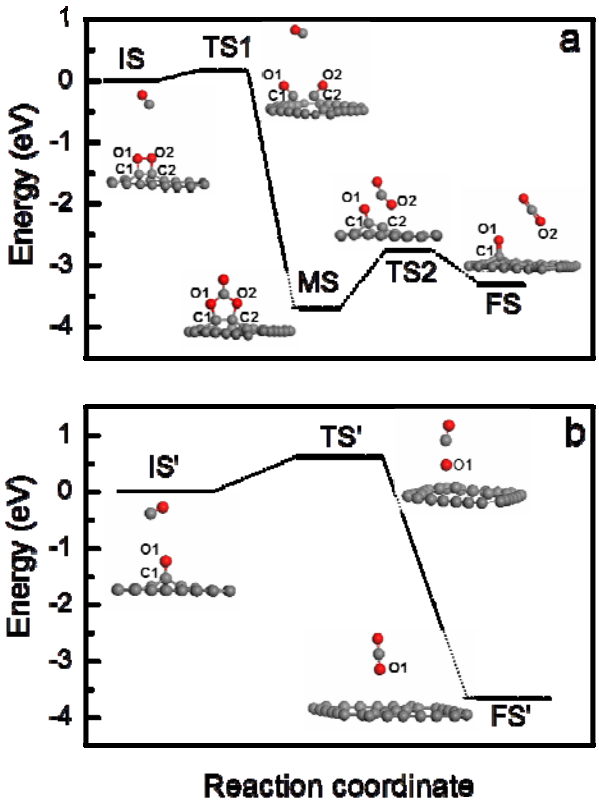

Fig. 3 Configurations of each state and minimum energy profiles for CO oxidation reaction on graphdiyne sheet along pathway II in ER mechanism, including initial state (IS), transition state (TS), intermediate state (MS), and final state (FS) for step 1, initial state (IS′), transition state (TS′), and final state (FS′) for step 2. Atomic color code: grey, carbon and red, oxygen.

We first considered the LH mechanism (Fig. S5, ESI). When CO and O_2 are coadsorbed on the graphdiyne sheet (IS in Fig. S5, ESI), the carbon atom of the adsorbed CO molecule starts to approach

one oxygen atom in the adsorbed O_2 molecule to reach the transition state (TS in Fig. S5, ESI). The O–O bond length of the adsorbed O_2 is dissociated to 1.67 Å, and the distance of C in CO and O in O_2 decreases from 3.33 to 1.93 Å. This is an endothermic process with an energy barrier of ~1.03 eV. Passing over the TS, O–O is continually elongated to 3.91 Å, and finally a CO_2 molecule is formed, leaving an atomic O adsorbed on graphidyne sheet (FS in Fig. S5, ESI). During the CO oxidation via the LH mechanism, no OOCO intermediate was found. Considering the relative high energy barrier of the CO_2 formation via the LH mechanism (~1.03 eV. Note that the energy barrier in ER mechanism is ~0.18 eV in the rate-limiting step, please refer to the following discussion for details), we will focus on the ER mechanism in the following sections.

In ER mechanism, there are two possible pathways (pathway I and II) of CO oxidation.[54] The pathway I is considered through the reaction: $O_{2(ad)} + CO_{(gas)} \rightarrow O_{(ad)} + CO_{2(gas)}$ (step 1. The $CO_{(gas)}$ directly extracts one O atom of adsorbed $O_{2(ad)}$), proceeding with $CO + O_{(ad)} \rightarrow CO_{2(gas)}$ (step 2). The pathway II is considered via the interaction of the isolated CO and atomic O as following: $O_{2(ad)} + CO_{(gas)} \rightarrow O_{(ad)} + O_{(ad)} + CO_{(gas)} \rightarrow O_{(ad)} + CO_{2(gas)}$ (step 1. After dissociation of adsorbed $O_{2(ad)}$, the $CO_{(gas)}$ directly extracts one adsorbed $O_{(ad)}$ atom), proceeding with $CO_{(gas)} + O_{(ad)} \rightarrow CO_{2(gas)}$ (step 2). Our calculations indicated that the energy barrier of pathway I is as high as 3.41 eV (for step 1, Fig. S6, ESI), suggesting that CO oxidation is not favorable undergoing through pathway I. Therefore, the reaction mechanism on the pathway II will be discussed in detail.

Fig. 3 shows the optimized configurations at various steps of the CO oxidation on graphdiyne sheet and the energy profile of MEP (the minimum energy pathway) along pathway II in ER mechanism. To search the MEP for CO oxidation with O_2, the most stable O_2 adsorption configuration was selected as the initial state (IS), where CO is physisorbed near O_2 molecule with an intermolecular distances of 4.43 Å (the distance of C in CO and O1 in adsorbed O_2, Fig. 3a). In this configuration, the bond length of C–O in CO and O–O in adsorbed O_2 is 1.15 and 1.56 Å, respectively. The O–O bond in the adsorbed O_2 molecule is elongated by 27.9% in comparison with that in the isolated O_2, suggesting that the adsorbed O_2 is active enough to oxidize the CO via the ER mechanism. In the reaction pathway, CO starts to

approach the adsorbed and activated O_2 to reach the transition state (TS1), meanwhile, the O–O bond is elongated to 3.40 Å (the distance between O1 and O2), implying the breakage of O–O bond in the adsorbed O_2 and the formation of the two atomic O adsorbed on graphdiyne sheet. The distance between the C in CO molecule and the formed atomic O decreases to ~3.62 Å. This step needs to overcome an energy barrier of ~0.18 eV due to the breakage of O–O bond. With CO continuing to approach, a metastable carbonate-like intermediate state (MS) is generated. This is nearly the same as the reaction of CO with O_2 on surface of Au and Ag,[55-57] and also quite similar to the case of Fe-embedded graphene.[23] The process of MS formation is exothermic one by 3.68 eV. The bond length of the new formed C1–O1 and C2–O2 bonds in MS is 1.40 and 1.42 Å, respectively. As the reaction proceeding, MS goes through an endothermic dissociation crossing a relatively high energy barrier of ~0.94 eV for the cost of the breakage of C2–O2 bond (breakage of C2–O2 bond is prior to C1–O1 bond as indicated by their bond length) and the generation of the first CO_2 molecule and one atomic O_{ad} adsorbed on graphdiyne surface (TS2). The distance of O2 (in the generated CO_2 molecule) to C2 is 2.07 Å, and the bond length of C1–O1 bond decreases to 1.29 Å from 1.40 Å. The generated CO_2 molecule drifts away from graphdiyne sheet with a distance of ~4.20 Å (from the O2 in CO_2 molecule to the graphdiyne plane), implying the dissociation of CO_2 from graphdiyne surface. Afterwards, the bond length of C1–O1 bond further decreases to 1.26 Å and the system reaches a final state (FS) with the atomic O strongly adsorbed on graphdiyne sheet. Note that the release of the CO_2 molecule from the surface of graphdiyne is easy because interaction between CO_2 and graphdiyne is very weak ($E_{ad}(CO_2)$ = –0.04 eV) and the exothermicity (0.53 eV) of the process can sufficiently overcome the adsorption energy of CO_2.

Then, the second step for CO oxidation with the atomic O_{ad} along the ER mechanism involves that the adsorbed atomic O_{ad} reacts with another CO molecule (IS′) to produce the second CO_2 molecule (FS′) with energy barrier of 0.64 eV (TS′) for the breakage of C1–O1 bond (Fig. 3b). In TS′, the distance between the C in CO molecule and O_{ad} (O1) is ~1.42 Å, however, the distance of O1 to graphdiyne plane is ~1.80 Å. Desorption of the generated CO_2 molecule from graphdiyne surface is an

energy favorable process. After the CO_2 molecule drifts away, the saddle-shaped graphdiyne recovers its original shape and is ready for the next reaction cycle.

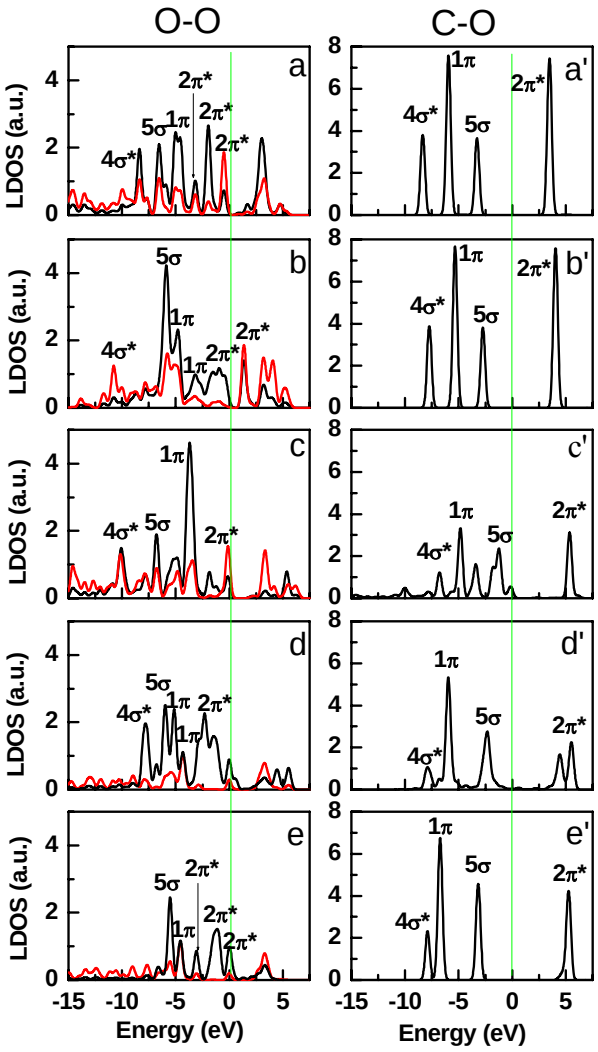

Fig. 4 LDOS projected onto O–O (a–e) and C–O (a′–e′) for each state of CO oxidation at graphdiyne sheet in step (1) of the ER mechanism. (a, a′), (b, b′), (c, c′), (d, d′), and (e, e′) correspond to IS, TS1, MS, TS2, and FS, respectively, as described in Fig. 3a. Red lines in (a–e) represent LDOS projected onto C atoms in graphdiyne sheet bound with the adsorbed O_2 or atomic O. The green line represents the Fermi level.

To evaluate the catalytic activity of graphdiyne to CO oxidation, we compared the energy barrier of CO oxidation on graphdiyne surface with those obtained on the surface of some transition metals and metal-decorated carbon materials. The energy barrier of dissociation of O_2 on graphdiyne is ~0.18 eV, which is much lower than those on Au (111) (1.97 eV),[58] Au (211) (0.65 eV),[56] Au (221) (0.59 eV),[56]

Pt/Si-graphene (0.72 eV),[59] Fe-embedded graphene (0.58 eV),[23] and Fe-graphene oxide (0.61 eV),[24] and slightly lower than that on W (111) (0.26 eV).[54] The value of the energy barrier of generation of the first CO_2 molecule (0.938 eV) is also lower than that on Ir (100) (1.56 eV),[60] and Fe-embedded graphene (1.11 eV),[23] and comparable to that found on Fe-graphene oxide (0.93 eV)[24] and W (111) (0.92 eV).[54] The energy barrier of the generation of the second CO_2 molecule in step 2 (0.64 eV) is also much smaller than those on Ru(0001) (1.20–1.68 eV),[61] Rh(111) (1.13–1.17 eV),[19,58] W(111) (0.99 eV),[54] W_{10} cluster (1.0 eV),[54] Pt (111) (0.74–1.0 eV),[19,61] and Pd (111) (0.91–1.05 eV).[19,61] These results demonstrate that the oxidation of CO on graphdiyne is relative more favorable with a low energy barrier.

To understand deeply the origin of the high catalytic activity of graphdiyne towards CO oxidation, we investigated the electronic structures of each step in ER reaction progresses. Fig. 4 depicts the LDOS projected onto O–O (Fig. 4a-e) and C–O bonds (Fig. 4a′-e′), together with the LDOS of the C atoms in graphdiyne bound with O_2 and CO molecules in the IS, TS1, MS, TS2, and FS of the ER mechanism of CO oxidation (see Fig. 3 for the geometric configuration of each state). Upon O_2 adsorption on graphdiyne (IS), the antibonding O_2-2π* orbital is occupied and becomes broad and split (Fig. 4a), compared with that of isolated O_2 (note that the LDOS of the isolated O_2 is depicted Fig. 1h), caused by remarkable electron transfer from graphdiyne to the adsorbed O_2. Moreover, there are some overlaps between orbitals of the adsorbed O_2 and graphdiyne, indicative of the effective interaction between graphdiyne sheet and the adsorbed O_2. This interaction leads to an obvious elongation of O–O bond. However, the LDOS of C–O in IS (Fig. 4a′) is almost the same as that of isolated CO (the LDOS of the isolated CO is depicted Fig. 1g), suggesting the adsorption of CO on graphdiyne is very weak. From IS to TS1, O_2-1π and O_2-2π* orbitals (Fig. 4b) gradually turn to be more broad and pass the Fermi level, implying the O–O bond is weakened and elongated, and the adsorbed O_2 molecule dissociates to atomic O adsorbed on graphdiyne sheet. In addition, there is slight shift-up of O_2-2π* orbital, suggesting that the binding strength of atomic O on graphdiyne is strong. Meanwhile, 5σ orbital of C–O bond in TS1 becomes slight broad and moves toward the Fermi level direction (Fig. 4b′), indicative of the enhancement of the interaction between the CO and graphdiyne as CO gradually

approaching to graphdiyne sheet. In the MS, the strong hybridization between 1π, 5σ, and 4σ* orbitals of O_2 and the orbital of graphdiyne can be observed below the Fermi level (Fig. 4c). The 5σ orbital of C–O bond expands and is slightly elevated to be near the Fermi level (Fig. 4c′) due to the interaction between O_2 and CO as indicated by the decrease of distance between C in CO and O in O_2 and the formation of the carbonate-like intermediate. In TS2, the C–O bond in intermediate is further elongated as evidenced by a descent in the LDOS of both O–O and C–O bond (Fig. 4d, d′), suggesting that the generated CO_2 is adsorbed weakly on graphdiyne sheet and can be easily desorbed from graphdiyne sheet. In FS, LDOS of the product are almost the same as those of the isolated CO_2 and the adsorbed atomic O, indicating desorption of the generated CO_2 and remaining of only an adsorbed atomic O on graphdiyne sheet.

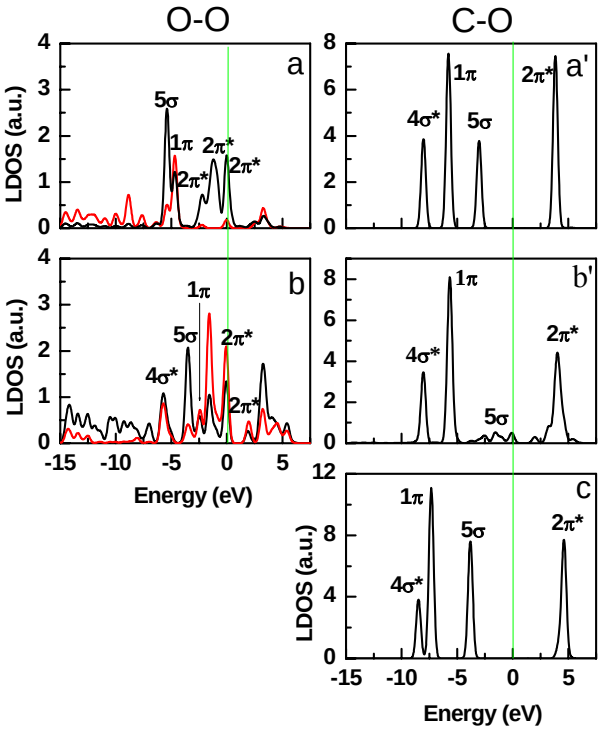

Fig. 5 LDOS projected onto O–O (a–b), C–O (a′–b′), and CO_2 (c) for each state of step 2 in CO oxidation at graphdiyne sheet. (a, a′), (b, b′), and (c) corresponds to IS′, TS′ and FS′ state as described in Fig. 3b, respectively. Red line represents LDOS projected onto C atoms in graphdiyne sheet bound with the adsorbed O_2 or atomic O. The green line represents the Fermi level.

We also analyzed the LDOS projected onto O–O and C–O bonds, and the C atoms in graphdiyne for each state of CO oxidation in step 2 along the ER mechanism (Fig. 5). In IS′, the 2π* orbital of atomic

O is wide and overlaps with the orbital of graphdiyne (Fig. 5a); the LDOS of C–O remains almost unchangeable compared to that of isolated CO molecule (Fig. 5a′), indicating that the atomic O is strongly adsorbed on graphdiyne while CO is weakly adsorbed on graphdiyne sheet. The $2\pi^*$ orbital of O is partially occupied in TS′ configuration (Fig. 5b), leading to weaken the C1–O1 bond. The 5σ orbital of CO in TS′ is in occupation state near the Fermi level (Fig. 5b′), indicative of the interaction of the atomic O with the CO molecules. The LDOS of the generated CO_2 (Fig. 5c) is similar to the isolated CO_2, implying desorption of the generated CO_2 molecule from graphdiyne. After that, graphdiyne is ready for the next reaction cycle.

In general, the CO oxidation with a reaction barrier of less than 0.5 eV is expected to occur at the ambient temperature. The reaction barrier in the rate-limiting step for CO oxidation on graphdiyne sheet is as low as 0.18 eV, implying the oxidation of CO is likely to proceed rapidly via ER mechanism at room temperature. Moreover, the planar nature of raphdiyne with high surface area ensures its high catalytic efficiency and activity in reaction progresses. Thus, graphdiyne can be a good, metal-free, and low-cost catalyst for CO oxidation undergoing at low temperature and can be used in fuel cell with high CO-tolerance.

4. Conclusions

We have used DFT calculations to demonstrate that graphdiyne is a good, metal-free, and low-cost catalyst for low-temperature CO oxidation. The simulation results indicate that the adsorption of O_2 prevails over CO adsorption on graphdiyne sheet; the reaction of CO oxidation on graphdiyne proceeds via ER mechanism including breakage of the adsorbed O–O bond, formation of the metastable carbonate-like intermediate state, and the creation of CO_2 molecules with a decrease in the energy of the system and the energy barrier of as low as 0.183 eV in the rate-limiting step. This work should open a new avenue to develop carbon nanomaterials used in environment- and energy-related fields.

Acknowledgements

This work is supported by NSFC (21175067, 21273117, 21375063, and 21335004), NSF of Jiangsu Province (BK2011779), the Program for Outstanding Innovation Research Team of Universities in Jiangsu Province, and the Priority Academic Program Development of Jiangsu Higher Education Institutions.

References

1 H. A. Gasteiger and N. M. Marković, *Science*, 2009, **324**, 48-49.

2 V. R. Stamenkovic, B. Fowler, B. S. Mun, G. Wang, P. N. Ross, C. A. Lucas and N. M. Marković, *Science*, 2007, **315**, 493-497.

3 Y. Hu, P. Wu, Y. Yin, H. Zhang and C. Cai, *Appl. Catal. B: Environmental*, 2012, **111-112**, 208-217.

4 P. Wu, H. Zhang, Y. Qian, Y. Hu, H. Zhang and C. Cai, *J. Phys. Chem. C*, 2013, **117**, 19091-19100.

5 Y. Hu, Q. Shao, P. Wu, H. Zhang and C. Cai, *Electrochem. Commun.*, 2012, **18**, 96-99.

6 C.-T. Hsieh, Y.-S. Chang and K.-M. Yin, *J. Phys. Chem. C*, 2013, **117**, 15478-15486.

7 S.-I. Choi, S. Xie, M. Shao, J. H. Odell, N. Lu, H.-C. Peng, L. Protsailo, S. Guerrero, J. Park, X. Xia, J. Wang, M. J. Kim and Y. Xia, *Nano Lett.*, 2013, **13**, 3420-3425.

8 X. Wang, Y. Orikasa, Y. Takesue, H. Inoue, M. Nakamura, T. Minato, N. Hoshi and Y. Uchimoto, *J. Am. Chem. Soc.*, 2013, **135**, 5938-5941.

9 Y. Hu, P. Wu, H. Zhang and C. Cai, *Electrochem. Acta*, 2012, 85, 314-321.

10 S. E. Mason, I. Grinberg and A. M. Rappe, *J. Phys. Chem. C*, 2008, **112**, 1963-1966.

11 G. Papoian, J. K. Nørskov and R. A. Hoffmann, *J. Am. Chem. Soc.*, 2000, **122**, 4129-4144.

12. P. Rodríguez, A. A. Koverga and M. T. M. Kopper, *Angew. Chem. Int. Ed.*, 2010, **49**, 1241-1243.

13. W. Gao, J. E. Mueller, Q. Jiang and T. Jacob, *Angew. Chem. Int. Ed.*, 2012, **51**, 9448-9453.

14. P. Rodríguez, Y. Kwon, M. T. M. Kopper, *Nature Chem.*, 2012, **4**, 177-182.

15 L. Chen, B. Chen, C. Zhou, J. Wu, R. C. Forrey and H. Cheng, *J. Phys. Chem. C*, 2008, **112**, 13937-13942.

16 S. H. Oh and G. G. Hoflund, *J. Catal.*, 2007, **245**, 35-44.

17 D. I. Kochubey, S. N. Pavlova, B. N. Novgorodov, G. N. Kryukova and V. A. Sadykov, *J. Catal.*, 1996, **161**, 500-506.

18 M. Haruta, N. Yamada, T. Kobayashi, H. Kageyama, M. J. Genet and B. Delmon, *J. Catal.*, 1993, **144**, 175-192.

19 X.-Q. Gong, Z.-P. Liu, R. Raval and P. Hu, *J. Am. Soc. Chem.*, 2004, **126**, 8-9.

20 G. Lanzani, A. G. Nasibulin, K. Laasonen and E. I. Kauppinen, *Nano Res.*, 2009, **2**, 660-670.

21 W. Xue, Z.-C. Wang, S.-G. He and Y. Xie, *J. Am. Chem. Soc.*, 2008, **130**, 15879-15888.

22 X. Xie, Y. Li, Z.-Q. Liu, M. Haruta and W. Shen, *Nature*, 2009, **458**, 746-749.

23 Y. Li, Z. Zhou, G. Yu, W. Chen and Z. Chen, *J. Phys. Chem. C*, 2010, **114**, 6250-6254.

24 F. Li, J. Zhao and Z. Chen, *J. Phys. Chem. C*, 2012, **116**, 2507-2514.

25 E. H. Song, Z. Wen and Q. Jiang, *J. Phys. Chem. C*, 2011, **115**, 3678-3683.

26 D. J. D. Durbin and C. Malardier-Jugroot, *J. Phys. Chem. C*, 2011, **115**, 808-815.

27 M. Jahan, Q. L. Bao and K. P. Loh, *J. Am. Chem. Soc.*, 2012, **134**, 6707-6713.

28 H. Liu and J.Y. Lee, *J. Phys. Chem. C*, 2012, **116**, 3034-3041.

29 D. Pan, M. Ombaba, Z. Y. Zhou, Y. Liu, S. Chen and J. Lu, *ACS Nano*, 2012, **6**, 10720-10726.

30 Y. Zhao, L. Yang, S. Chen, X. Wang, Y. Ma, Q. Wu, Y. Jiang, W. Qian and Z. Hu, *J. Am. Chem. Soc.*, 2013, **135**, 1201-1204.

31 K. Gong, F. Du, Z. Xia, M. Durstock and L. Dai, *Science*, 2009, **323**, 760-764.

32 L. Yang, S. Jiang, Y. Zhao, L. Zhu, S. Chen, X. Wang, Q. Wu, J. Ma, Y. Ma and Z. Hu, *Angew. Chem., Int. Ed.*, 2011, **50**, 7132-7135.

33 P. Wu, P. Du, H. Zhang and C. Cai, *J. Phys. Chem. C*, 2012, **116**, 20472-20479.

34 G. Li, Y. Li, H. Liu, Y. Guo, Y. Li and D. Zhu, *Chem. Commun.*, 2010, 46, 3256-3258.

35 J. P. Perdew, K. Burke and M. Ernzerhof, *Phys. Rev. Lett.*, 1996, **77**, 3865-3868.

36 H. J. Monkhorst and J. D. Pack, *Phys. Rev. B*, 1976, **13**, 5188-5192.

37 B. Delley, *J. Chem. Phys.*, 1990, **92**, 508-517.

38 B. Delley, *J. Chem. Phys.*, 2000, **113**, 7756-7764.

39 K. Srinivasu and S. K. Ghosh, *J. Phys. Chem. C*, 2012, **116**, 5951-5956.

40 M. Long, L. Tang, D. Wang, Y. Li and Z. Shuai, *ACS Nano*, 2011, **5**, 2593-2600.

41 N. Narita, S. Nagai, S. Suzuki and K. Nakao, *Phys. Rev. B*, 2000, **62**, 11146-11151.

42 H. X. Bu, M. Z. Zhao, H. Y. Zhang, X. P. Wang, Y. Xi and Z. H. Wang, *J. Phys. Chem. A*, 2012, **116**, 3934-3939.

43 M. D. Morse, *Chem. Rev.*, 1986, **86**, 1049-1109.

44 B. G. Johnson, P. M. W. Gill and J. A. Pople, *J. Chem. Phys.*, 1993, **98**, 5612-5626.

45 S. Chrétien, S. K. Buratto and H. Metiu, *Curr. Opin. Solid State Mater. Sci.*, 2007, **11**, 62-75.

46 L. Zhang and Z. Xia, *J. Phys. Chem. C*, 2011, **115**, 11170-11176.

47 J. K. Nørskov, J. Rossmeisl, A. Logadottir, L. Lindqvist, J.R. Kitchin, T. Bligaard and H. Jónsson, *J. Phys. Chem. B*, 2004, **108**, 17886-17892.

48 M. C. S. Escaño, H. Nakanishi and H. Kasai, *J. Phys. Soc. Jpn.*, 2009, **78**, 064603 (8 pages).

49 M. A. Petersen, S. J. Jenkins and D. A. King, *J. Phys. Chem. B*, 2006, **110**, 11962-11970.

50 P. B. Balbuena, D. Altomare, L. Agapito and J. M. Seminario, *J. Phys. Chem. B*, 2003, **107**, 13671-11680.

51 C. Liu, Y. Tan, S. Lin, H. Li, X. Wu, L. Li, Y. Pei and X. C. Zeng, *J. Am. Chem. Soc.*, 2013, **135**, 2583-2595.

52 Y.-H. Lu, M. Zhou, C. Zhang and Y.-P. Feng, *J. Phys. Chem. C*, 2009, **113**, 20156-20160.

53 B. Hammer and J. K. Nørskov, *Adv. Catal.*, 2000, **45**, 71-129.

54 M. H. Weng and S. P. Ju, *J. Phys. Chem. C*, 2012, **116**, 18803-18815.

55 H.-T. Chen, J.-G. Chang, S.-P. Ju and H.-L. Chen, *J. Comput. Chem.*, 2010, **31**, 258-265.

56 Z. P. Liu, P. Hu and A. Alavi, *J. Am. Chem. Soc.*, 2002, **124**, 14470-14479.

57 H. Y. Kim, S. S. Han, J. H. Ryu and H. M. Lee, *J. Phys. Chem. C*, 2010, **114**, 3156-3160.

58 H.-Y. Su, M.-M. Yang, X.-H. Bao and W.-X. Li, *J. Phys. Chem. C*, 2008, **112**, 17303-17310.

59 Y. Tang, Z. Yang, X. Dai, D. Ma and Z. Fu, *J. Phys. Chem. C*, 2013, **117**, 5258-5268.

60 I. A. Erikat, B. A. Hamad and J. M. Khalifeh, *Phys. Status. Solidi B*, 2011, **248**, 1425-1430.

61 A. Eichler and L. Hafner, *Phys. Rev. B*, 1999, **59**, 5960-5967.